Functional differentiation of dorsal and ventral posterior parietal cortex of the rat: Implications for controlled and stimulus driven attention

Yang, Fang-Chi[1], Dokovna, Lisa B. [1], and Burwell, R.D.[1,2]

[1] Cognitive, Linguistic & Psychological Sciences, Brown University, Providence, Rhode Island 02912, USA. [2] Department of Neuroscience, Brown University, Providence, Rhode Island 02912, USA.

Running head**:** Functional differentiation in rat posterior parietal cortex

Email addresses:

fang-chi_yang@brown.edu

lisa_dokovna@alumni.brown.edu

rebecca_burwell@brown.edu

Corresponding author: Rebecca D. Burwell, Ph.D.

The posterior parietal cortex (PPC) is important for visuospatial attention. The primate PPC shows functional differentiation such that dorsal areas are implicated in top-down, controlled attention, and ventral areas are implicated in bottom-up, stimulus driven attention. Whether the rat PPC also shows such functional differentiation is unknown. Here, we address this open question using functional neuroanatomy and *in vivo* electrophysiology. Using conventional tract-tracing methods, we examined connectivity with other structures implicated in visuospatial attention including the lateral posterior nucleus of the thalamus (LPn) and postrhinal cortex (POR). We showed that the LPn projects to the entire PPC, preferentially targeting more ventral areas. All parts of the PPC and POR are reciprocally connected with the strongest connections evident between ventral PPC and caudal POR. Next, we simultaneously recorded neuronal activity in dorsal and ventral PPC as rats performed a visuospatial attention task that engages in both bottom-up and top-down attention. Previously, we provided evidence that the dorsal PPC is engaged in multiple cognitive process including controlled attention (Yang et al. 2017). Here, we further showed that ventral PPC cells respond to stimulus onset more rapidly than dorsal PPC cells providing evidence for a role in stimulus-driven, bottom-up attention.

Key words: perception, action, navigation, default mode network, postrhinal cortex

The posterior parietal cortex (PPC) in humans, monkeys, and rodents is implicated in visuospatial attention (Colby and Goldberg 1999; Bucci 2009; Petersen and Posner 2012). In the monkey, a primary target of the PPC is the medial temporal lobe, including the hippocampal formation and the parahippocampal cortex (PHC) (Cavada and Goldman-Rakic 1989; Suzuki and Amaral 1994a; Suzuki 1996; Kravitz et al. 2011). The rodent homolog of the primate PHC is the postrhinal cortex (POR) (Burwell et al. 1995). Some evidence suggests the POR, which has reciprocal connections with the PPC, supports attentional monitoring for the purpose of detecting changes in the environmental context (Bucci and Burwell 2004; Furtak et al. 2012). Both the POR and PPC are interconnected with the lateral posterior nucleus of the thalamus (LPn), part of which is homologous with the primate visual pulvinar (Agster et al. 2016; Tomás Pereira et al. 2016; Baldwin et al. 2017; Kaas and Baldwin 2019). Parts of the LPn in rats and the pulvinar in primates are included in circuits that support visual attention (Reep and Corwin 2009; Saalmann and Kastner 2011; Yang and Burwell 2020).

A number of anatomical studies have addressed connections among the PPC, POR and LPn in rats. Some earlier studies focused entirely on the dorsal portion of the PPC, about 3.5-5.0 mm posterior to bregma and 1.5-5.0 lateral from the midline (Chandler et al. 1992; Reep et al. 1994; Furtak et al. 2007; Nakamura et al. 2015). It now appears that the border of the rodent PPC might extend ventrally to adjacent regions that have sometimes been included in visual association cortex. Two recent studies concluded that the dorsomedial secondary visual cortex, an adjacent area posterior to the PPC, exhibits patterns of neuronal connectivity, and possibly functions, similar to those of the PPC (Wilber, Clark, Demecha, et al. 2014; Wilber, Clark, Forster, et al. 2014). Consequently, more recent anatomical studies included these adjacent regions in the delineation of PPC (Agster *et al.* 2016; Olsen and Witter 2016; Tomás Pereira *et al.* 2016; Olsen et al. 2017). To better understand the anatomy and function of the PPC as a

whole, the anatomical connections of ventral part of the PPC (VPPC) need to be further examined with special attention to identifying the border between the VPPC and the adjacent secondary visual cortex.

Most electrophysiological studies of the rodent PPC, including our previous work, primarily focused on the dorsal portion of the PPC (Chen et al. 1994; Nitz 2009, 2012; Whitlock et al. 2012; Yang *et al.* 2017). The dorsal PPC (DPPC) in rodents is implicated in attention, spatial navigation, and visually-guided actions (Broussard et al. 2006; Bucci 2009; Nitz 2014). We previously reported that DPPC cells signaled stimulus onset, target selection, and task-relevant spatial locations when rats performed a visuospatial attention task (Yang *et al.* 2017). This single-sided visuospatial attention task was adapted from the five-choice serial reaction time (5CSRT) task developed to assess visuospatial attention and prefrontal (executive) function (Carli et al. 1983; Bari et al. 2008). Rats were required to visually monitor locations in space in order to in order to detect visual stimuli presented briefly on the floor of a maze at one target location randomly chosen from three. Rats made a selection by approaching the previously illuminated target location in order to obtain a food reward. Neuronal correlates of DPPC in this prior study provided evidence for the involvement of the DPPC in visuospatial attention and in the top-down control of the translation of perception to action. Similar to a number of other rodent studies of the PPC, we did not record in the ventral PPC. In the present study, we recorded simultaneously in the DPPC and the VPPC.

Human studies indicate that subregions of the PPC are functionally differentiated such that the more dorsal part is more involved in top-down attention and the more ventral part is more involved in bottom-up attention (Corbetta et al. 2000; Corbetta and Shulman 2002; Shomstein 2012). There is less evidence for top-down and bottom-up differentiation in the non-human primate literature. There is, however, evidence for functional differentiation of monkey PPC subregions with respect to different types of attention (Cook and Maunsell 2002; Caspari et

al. 2017), and there is evidence for functional similarity of dorsal PPC across humans and monkeys (Cook and Maunsell 2002; Caspari *et al.* 2017). It may be that strong electrophysiological evidence of a top-down/bottom-up differentiation in subdivisions of monkey PPC is lacking because electrophysiological recordings in the monkey PPC related to visual attention have focused primarily on the lateral intraparietal cortex (LIP) (Bisley and Goldberg 2003; Buschman and Miller 2007; Gottlieb 2007). In any case, the extent to which functional differentiation exists in the rodent PPC and whether or not such functional differentiation maps onto the primate PPC have not been previously addressed. Addressing such open questions would clarify the extent to which rodent models can be used to better understand visuospatial attention circuits in the primate brain.

In the present study, we first characterized the topography of the anatomical connections of the DPPC and VPPC with the LPn and the POR. Then, to further test the hypothesis of functional differentiation among PPC subdivisions, we simultaneously recorded neuronal activity in the rat DPPC and VPPC during performance on the visuospatial attention (VSA) task. We adapted the VSA task from the five-choice serial reaction time task (Carli *et al.* 1983) for use in our floor projection maze apparatus (Furtak et al. 2009; Jacobson et al. 2014). The VSA task engages multiple cognitive processes, including visual perception, decision-making, and reward learning. This allows us to investigate both bottom-up, saliency-driven attention and top-down, controlled attention guided by task-relevant signals (Yang *et al.* 2017; Yang and Burwell 2020). Here, we provide both neuroanatomical and electrophysiological evidence for our hypothesis that the DPPC and VPPC are functionally differentiated in the rat brain.

Methods

Nomenclature

The PPC in the rat is a narrow strip of cortex located between somatosensory and visual regions (Figure 1). The rostral aspect of the region originates on the dorsal surface of the

brain and extends laterally and then ventrolaterally. The dorsal area, located from 3.2 to 5.0 mm caudal to bregma and from 1.5 to 5.0 mm lateral to the midline is much better studied than the ventral area. This may have resulted because two prominent atlases show better agreement on the location of the dorsal PPC than on the caudal portion (Swanson 2004; Paxinos and Watson 2014). The dorsal portion of the PPC is known to be interconnected with frontal regions (Reep *et al.* 1994). The ventrolateral area is more robustly interconnected with the POR than the dorsal area (Burwell and Amaral 1998a).

Figure 1

The dorsal PPC, which we collectively refer to as DPPC, includes MPtA, LPtA, part of PtPD, and part of PtPR; whereas, the ventrolateral area, VPPC, collectively includes part of PtPD, part of PtPR, and PtPC (Figure 1). This nomenclature is consistent with most published studies as well as with Paxinos and Watson (2014) and Swanson (Swanson 2018). Based on cytoarchitectonic and connectional criteria (present study; Agster *et al.* 2016; Tomás Pereira *et al.* 2016), we placed the caudal border VPPC at ~6.3 mm caudal to bregma, which is between the caudal borders according to Paxinos and Watson (2014) and Swanson (Swanson 2018). The connections with POR include this adjacent area.

Figure 2

The POR borders are from Burwell (2001). A convenient and fairly reliable landmark for the rostral border of the POR is the caudal end of the angular bundle, adjacent to the caudal border of PER area 36. The POR is bordered ventrally by the medial EC and lies dorsal to the rhinal sulcus. The most rostral extent of the POR can be divided into two subfields, a dorsal POR (PORd) and ventral POR (PORv) based on the cytoarchitecture (Burwell 2001). Our

analysis also included a rostral/caudal division of the POR for the purpose of observing a topographic map of interconnections with the LPn and the PPC.

For nomenclature and coordinates of the LPn, we used Paxinos and Watson (Paxinos and Watson 2014). Based on cytoarchitecture, the LPn is subdivided into the nucleus lateralis posterior pars rostromedialis (LPMR), nucleus lateralis posterior pars caudomedialis (LPMC), and the nucleus lateralis posterior pars lateralis (LPL, Figure 2). Six coronal levels are shown in Figure 2A-F, with an overhead view of the nuclei shown in Figure 2G. The rostral end of the LPMR appears medial to the nucleus lateralis dorsale pars dorsomedialis (LD) and lateral to centrolateral nucleus (Takahashi 1985). The LPMR is bordered laterally by the LPL and dorsally by the emerging LPMC. The LPMC emerges dorsal to the caudal tail of the LPMR, and is bordered medially by the anterior pretectal nucleus and laterally by the LPL. The caudal portion of LPMC is bordered dorsal-medially by the nucleus of the optic tract and ventral medially by the olivary pretectal nucleus. The LPL lies medial to the intramedullary thalamic area and lateral to the LPMR and LPMC. The LPL is further subdivided into the pars rostralis (LPLR) and pars caudalis (LPLC) based on its connectivity. LPLC, a narrower caudal portion of the LPL, receives input from the superficial layers of the ipsilateral SC, whereas LPLR receives no collicular input, but does receive input from cortical areas 17 and 18 (Takahashi 1985). This border, however, is not distinct based off of cytoarchitecture, but a working division can be used, where LPLR ends with the appearance of the rostral limit of LPMC. Subnuclei were identified and confirmed by comparing the gold intensified BDA sections with the corresponding Nissl-stained sections. The subnuclei of the LPn are known to have a differential neuronal morphology, which is identifiable using cytoarchitecture (Takahashi 1985). Nomenclature and abbreviations for all regions are shown in Table 1.

Table 1

Anatomical Methods

Subjects

For the anatomical study, we used 16 male rats. Ten Sprague-Dawley rats (Harlan Laboratories, Houston, TX) weighing 300-400 grams received tracer injections in the POR. Data from these rats were previously reported (Burwell and Amaral 1998a; Agster and Burwell 2009, 2013; Agster *et al.* 2016; Tomás Pereira *et al.* 2016). However, we used these rats for new analyses that have not been reported in previous studies. An additional six Sprague-Dawley rats (Charles River Laboratories, Wilmington, MA) weighing 250-350 grams received injections in the LPn.

For the electrophysiological study, subjects were five male Long-Evan rats weighing about 300 g at the time of implantation (Charles Rivers Laboratories, Wilmington, MA). Prior to surgery rats were housed individually or in pairs with *ad libitum* access to food and water. Pair housed rats were separated following surgery. Following surgery, rats were individually housed in a temperature-regulated colony maintained on a 12:12 h light:dark cycle. Experiments were carried out in the light phase. All methods involving the use of live animals conformed to NIH guidelines and were approved by the appropriate Institutional Animal Care and Use Committee.

Surgery. Subjects that received POR injections were anesthetized by a 50 mg/kg intraperitoneal (i.p.) injection of sodium pentobarbital (n=10; Nembutal©, Abbott Laboratories, North Chicago, IL). Subjects that received LPn injections (n=6) were anesthetized with isoflurane (Isothesia, Butler Schein Animal Health, Dublin, OH). Anesthesia was induced with 3% isoflurane and maintained with 1.0 -2.5% isoflurane. One hour prior to surgical induction, these subjects received preoperative medications to control for possible respiratory problems, minimize stress from surgery, and as a prophylactic measure against seizures. These

medications included a 2 mg/kg intraperitoneal injection of Diazepam (Hospira, Inc., Lake Forest, IL), and subcutaneous (s.q.) injections of 5 mg/kg Carprofen (Pfizer Animal Health, New York, NY), 0.5 mg/kg Butorphanol tartrate (Fort Dodge Animal Health, Fort Dodge, IO), and 0.05 mg/kg Glyocpyrrolate (West Ward, Eatontown, NJ). Following anesthesia induction, rats were secured in a Kopf stereotaxic apparatus in the flat skull position, after which isoflurane was reduced to 1-2.5% for the remainder of the surgery. Body temperature was maintained during surgery at 37° C with a calibrated heating pad. The scalp was shaved and cleaned with a betadine swab, and the subject then received a s.q. injection of 0.1 ml lidocaine (Hospira, Inc., Lake Forest, IL). An incision was then made after a brief waiting period to expose the skull, with bregma and lambda readily visible. A craniotomy was made dorsal to the intended injection site and a small incision was made in the dura to allow smooth entry of the glass micropipette. Coordinates for target areas were according to Paxinos and Watson (Paxinos and Watson 2005) and Swanson (Swanson 2004).

Retrograde tracers used were either Fast Blue (FB; Dr. Illing, Gmbh and Co. Gross Umstadt, Germany) or Diamidino Yellow (DY; Dr. Illing, Gmbh and Co. Gross Umstadt, Germany), both of which are commonly used in long-term experiments as they are effectively transported retrogradely over long distances. Survival times were 7-14 days. FB and DY were pressure injected through a glass micropipette with tip diameter ranging from 60 to 90 μm, with an approximate injection rate of 30 nl/min. The FB injections were approximately 150 nl of a 3% solution in distilled H_2O, and the DY injections were approximately 200 nl of a 2% solution in distilled H_2O. Following the injection of the retrograde tracer, the micropipette was raised 100 μm, and then after a 10-min waiting period, was slowly raised 500 μm/min before being removed (Burwell and Amaral 1998a, 1998b). Cases are suffixed FB or DY to indicate tracer used.

Anterograde tracers used were either a 2.5% solution of Phaseolus vulgaris-leucoagglutinin (PHA-L; Vector Laboratories, Burlingame, CA) in 0.1 M phosphate-buffered saline (PBS), or a 10% solution of biotinylated dextran amine (BDA, 10K MW, Molecular Probes, Inc., Eugene, OR) in 0.1 M PBS. In the present study, anterograde tracers were delivered through glass micropipettes with tip diameters ranging from 5 µm to 15 µm by iontophoresis, with 4 µA of positive direct current (7 seconds on and 7 seconds off) for 8 -10 minutes. Similar to the retrograde injections, there was a 10-minute wait period following the injection, during which the micropipette remained stationary. The micropipette was then slowly raised and removed from the injection site. Upon completion of the injections, the craniotomy was filled with gel foam, and the scalp was sutured along the incision. Rats were observed for 1-2 hours following surgery, and were kept warm with a heating pad during recovery. After the rats could demonstrate the righting reflex, they were returned to the colony. Rats received 6 mg of Rimadyl in chow (Rodent MD'sTM, BioServ, Hudson, NH) for three days following surgery. Cases are suffixed P when PHA-L was the tracer and B when BDA was the tracer.

Tissue Processing. Rats recovered for 7 to 14 days following surgery to allow for optimal transport of the tracers. After the survival period, subjects with POR injections were deeply anesthetized prior to perfusion with a 35% solution of chloral hydrate. Subjects with LPn injections were anesthetized prior to perfusion with 1.0 ml Beuthanasia-D (Schering-Plough Animal Health Corp, Union, NJ). All rats for this study were transcardially perfused following a pH-shift procedure to maximize visualization of tracers, as described previously in Burwell and Amaral (1998a, 1998b). Rats were perfused at a flow rate of 30-35 ml/minute. Each subject's head was packed with ice for the duration of the procedure. Rats were perfused with room temperature saline for approximately 2 minutes, followed by 4% paraformaldehyde in 0.1 M sodium acetate buffer, pH= 6.5, at 4oC for 10 minutes. Perfusion solution was then switched to a 4% paraformaldehyde in 0.1 M sodium borate buffer, pH=9.5, for 15 minutes. Brains were

immediately removed from the skull, and post-fixed in 4% paraformaldehyde in 0.1 sodium borate buffer for 6-24 hrs at 4°C. Brains were then cryoprotected in 20% glycerol in 0.02 M potassium PBS (KPBS) solution, pH=7.4, for at least 24 hrs prior to sectioning. Brains were coronally sectioned at 30 µm on a freezing microtome and collected in five series for processing and storage. For each brain, one 1:5 series was collected in formalin for Nissl staining with 0.25 % thionin, one series was collected in KPBS for immunohistochemical processing for visualization of the anterograde tracer, and one series was collected in KPBS for fluorescent visualization of the retrograde tracer. Spare series were either collected in PBS and stored at 4° C or in tissue collecting solution (30% ethylene glycol, 25% glycerin, 25% PBS, and 20% dH_2O) and stored at -20°C.

PHA-L anterograde cases were visualized using a biotinylated secondary antibody with an avidin-biotin reaction, and intensified using osmium tetroxide and thiocarbohydrazide. Free floating sections were first blocked in 0.5% Triton-X (TX) with 5% normal goat serum (NGS) in 0.02 M potassium phosphate buffered saline (KPBS) for 2 hours at room temperature on a rotating plate. This was followed by a primary antiserum incubation for two days in rabbit anti-PHA-L (1:12000; Dako, Carpenteria, CA) with 0.3% TX-100 in 2% NGS in KPBS at 4° C on a rotating plate. Free-floating sections were then washed 3 × 10 minutes in 2% NGS in KPBS prior to incubation in the biotinylated secondary solution. Afterwards, sections were then incubated for one hour in biotinylated goat-anti-rabbit IgG (1:227; Vector Laboratories, Burlingame, CA) in 0.3% TX-100 with 2% NGS in KPBS. Sections then washed 2 × 10 minutes in 2% NGS in KPBS, and then incubated in the avidin-biotin complex (Super ABC Kit; Biomedia Corporation, Foster City, CA) for 45 mins. Following the ABC incubation, sections were washed 2 × 10 minutes in 0.02M KPBS and then returned to the biotinylated secondary solution for an additional 45 minutes. Next, sections were washed 2 × 10 minutes in 0.02M KPBS, and then returned to the ABC solution for an additional 30 minutes. Sections were washed 3 × 10-

minutes in 0.02M KPBS prior to the visualization step. For this step, tissue was incubated in 0.05% diaminobenzidine (DAB; Pierce, Tacoma, WA) and 0.04% H_2O_2 in KPBS for 5-10 min. Sections were then washed 3 × 10 minutes in 0.02 M KPBS prior to being mounted on gelatin-coated slides. After slides were allowed to dry, they were defatted in a 50% chloroform in 100% ethanol solution for one hour. Slides were then hydrated through graded alcohols for 2 minutes each, prior to 10-20 minutes incubation in 0.005% Osmium tetroxide in ddH_2O. Slides were then washed for 30 minutes in running tap water, and then incubated for 5-15 minutes in 0.05% thiocarbohydrazide in ddH_2O. Following a 30-minute rinse in running tap water, slides were transferred back to the original osmium solution for 10-30 minutes, with background staining determining the length of time for the incubation. Finally, slides were rinsed for 30-minutes in running tap water, dehydrated through graded alcohols, cleared in xylene, and coverslipped with DPX.

BDA anterograde cases were visualized using an avidin-biotin reaction with either the osmium tetroxide and thiocarbohydrazide protocol described above, or a gold chloride procedure for intensification. Free-floating sections were first washed 3 × 10 min in KPBS and pretreated with a 1% solution of TX-100 in KPBS for 1 hr. The sections were then incubated overnight at 4^{o}C in a solution of avidin reagent and stabilizer (1:25 and 1:50 dilutions, respectively; Super ABC Kit; Biomeda Corporation; Foster City, CA) in KPBS plus 0.1% solution of TX. Following 3 × 10 minutes washes in KPBS, sections were visualized using a 0.05% DAB with 0.04% H_2O_2 in KPBS procedure for 5-30 minutes at room temperature depending on the speed of the reaction. Afterwards, sections were washed in KPBS and mounted on gelatin coated or charged slides. Slides were allowed to dry overnight, were defatted in a 50% chloroform in 100% ethanol solution for one hour, and then were hydrated for two minutes each in a series of graded alcohols. BDA was visualized with a 45-minute incubation at 56^{o}C in 1% silver nitrate in dH_2O in the dark. Silver nitrate was neutralized with a 30% ammonium hydroxide

in dH_2O, and then slides were rinsed with running water for two minutes prior to a 10-minute incubation in 0.2% Gold chloride in dH_2O in the dark. Slides were again washed in running water for two minutes before the silver-gold complex was stabilized in a 5% solution of sodium thiosulfate in dH_2O for 10 minutes at 56°C. Finally, slides were rinsed for two minutes in running water, dehydrated through graded alcohols, cleared in xylene, and coverslipped with DPX.

Sections to be analyzed for fluorescent retrogradely labeled cells were mounted on gelatin-coated slides. Slides were then dried for 2-4 hours in a vacuum desiccator at room temperature. Slides were dehydrated 2 × 10 minutes in 100% ethanol, cleared in xylene for 3 × 2 minutes, and coverslipped with DPX or Vectashield (Vector labs, Burlingame, CA).

Table 2

Quantification of Anterograde Labeling. Location of the injection site for the anterograde cases was identified using both bright-field and dark-field optics (Table 2). Some of these cases were previously used to describe the cortical, hippocampal, parahippocampal, and subcortical connections of the PER, POR and EC (Burwell and Amaral 1998b; Agster and Burwell 2009, 2013; Agster *et al.* 2016). For each case, a 1:5 series of 30 µm sections were examined using darkfield optics on a Nikon Optiphot-2 microscope (Tokyo, Japan) at a magnification of 4x and 10x. Using a methodology described in previous studies (Agster and Burwell 2009, 2013), for each section, density of fiber labeling for each region of interest was rated on a scale of 0-5: A score of zero indicated no fibers were present; 1, very weak fiber labeling; 2, weak; 3, moderate; 4, dense; and 5, very dense fiber labeling. The ratings were adjusted for each animal such that the full scoring range was used. A final estimate of anterograde label density was made for each target region and for each injection site by averaging across all sections.

Quantification of Retrograde Labeling. Location of the injection site for the retrograde cases was identified using bright-field optics (Table 2). These cases were previously used to describe the cortical, hippocampal, and parahippocampal connections of the PER, POR and EC (Burwell and Amaral 1998a, 1998b; Agster and Burwell 2013; Tomás Pereira *et al.* 2016). Using a methodology described in previous studies (Agster and Burwell 2013), the distribution of fluorescently labeled cells was plotted for a 1:10 series in the hemisphere ipsilateral side to the injection using Neurolucida 10 software (Microbrightfield Inc., Colchester, VT) interfaced with either a Nikon Optiphot-2 microscope or a Nikon E600 microscope (Tokyo, Japan) at a total magnification of 100X. For quantification, contours of the subcortical areas of interest and POR were drawn using Nissl-stained sections aligned with the brain contour drawn from the fluorescent retrograde sections. Neuroexplorer 10 analysis software (Microbrightfield Inc., Colchester, VT) was used to analyze each region of interest and the total number of labeled cells identified in the region of interest. Total cell numbers were first normalized for each section using a correction factor derived from the total number of labeled subcortical cells for each case. These cell counts were then multiplied by 10, to account for the 1:10 series, to estimate the total cell count in the region of interest. The volume of the region of interest was estimated by multiplying the total area of each section by 10 to account for the 1:10 series. The density of labeled cells for the region of interest was then calculated by dividing the estimated total number of cells by the estimated volume of the region of interest. Total cell counts were also used to calculate the percent of cells labeled in a subdivision, out of total number of cells in the region of interest.

Electrophysiological Methods

Apparatus. Behavioral training was conducted in the Floor Projection Maze, an apparatus that exploits the natural tendency of rats to attend to items located on or close to the ground and that permits automated control over visual stimuli (Furtak *et al.* 2009; Jacobson *et al.* 2014).

Essentially, the Floor Projection Maze is a horizontal rear projection screen positioned to allow back-projection of visual stimuli and to serve as a floor to any shaped arena (Figure 3A). The apparatus has a clear Plexiglas subfloor (147.32 cm × 111.80 cm and 1.25 cm thick) covered by Dual Vision Fabric (Da-Lite Screen Company, Warsaw, IN), a unity-gain flexible fabric designed for rear screen projection. A thin Plexiglas sheet (0.32 cm) covers the fabric for protection. Visual stimuli were projected onto the unity gain fabric from below the subfloor using an LCD projector (WT610 projector, NEC Corporation). In this experiment, the enclosure was a bowtie shaped arena for presentation of stimuli. Food reward (milk with various flavors) was delivered by two automated pumps (Med Associates, Inc, St. Albans, VT) to stainless steel food ports located at the middle region of the maze. Auditory stimuli were controlled by an automated auditory stimulus generator (ANL926, Med Associates, Inc.) and delivered through a speaker located above the maze.

The Floor Projection Maze was interfaced with three Windows PC systems, for location tracking, behavioral control, and neuronal data acquisition. Tracking was accomplished with a single camera using CinePlex Studio and Editor (v3.4.1) with Tracking and Basic Behavior modules (Plexon, Inc.). The position and body movements of the rat was recorded by calculating and tracking the centroid. Position data are analyzed online and saved in a datafile for offline analysis if needed. This system presented visual stimuli, collected behavioral data, and controlled delivery of reward based on the location of the rat. A Multichannel Acquisition Processor (MAP, Plexon Inc) and SortClient (Plexon, Inc) recorded real-time neuronal activity and behaviorally relevant event timestamps for later analysis. The MAP system was interfaced with the Med Associates system (DIG-713A SuperPort TTL Input Module and a DIG-726 SuperPort TTL Output module) used for controlling the projector, reward pumps, and audio signals.

Figure 3

Behavioral training. Rats were put on food schedules to maintain body weight at 85-90% of free feeding weight. After handling for at least 7 days, rats were habituated to the behavioral room for 10 min/day for three days. Rats were then shaped and trained in the VSA task. In the shaping sessions, rats first were trained in a 30-minute session to approach a visual target stimulus for a food reward (a drop of flavored milk). In the initial shaping sessions, we adopted an errorless shaping procedure such that when the rat moved toward one of the three locations in one side of the maze, the visual stimulus at that location would illuminate and a tone would signal a correct choice. A new trial on the other side of the maze would be initiated after the rat entered the reward area. After this initial shaping phase, rats were trained to stop in the ready position zone located in the middle of the bowtie shaped maze facing the side of the maze on which the target stimulus would be presented (Figure 3B). After a variable delay to wait for a stimulus presentation, a visual stimulus would illuminate in one of three randomly chosen locations. There was a short response window for rats to approach the location of the visual stimulus. Approach to the correct location was signaled by a brief tone and presentation of a drop of flavored milk as a food reward. If the rat approached an incorrect location, no reward was given, the trial was terminated, and a new trial would begin immediately. Rats were gradually trained in a series of steps culminating in the final parameters of the task. The duration for rats to stay in the ready position was gradually increased from 0.1 seconds to 1.6 seconds. Visual stimulus duration was gradually decreased from 20 seconds to 0.5 seconds. The response time window was decreased from 20 seconds to 5 seconds. In the final task, rats were required to stay in the ready position waiting for stimulus onset for a variable interval (1.2-1.6 seconds). A trial was defined as an omission trial when the rat did not make a selection during the 5-second response time window. Thus, during performance on the VSA task, the rat

was required to use stimulus-driven attention at the beginning of the trial and then to use previous knowledge to perform an appropriate behavioral choice resulting in an expected outcome. By outcome we mean whether the choice was correct and followed by reward or incorrect and not followed by reward.

The behavioral performance criterion for the end of training was 70-80% accuracy on the VSA task (chance is 33.33%). Rats in this study required 2-3 months of training to reach behavioral criterion on the final stage of the task. Hyperdrives were implanted after a rat reached behavioral criterion for 5 to 7 consecutive days. The response latencies were recorded for correct and incorrect trials and were calculated as follows: timestamp of selection – timestamp of start of stimulus onset. Latency to collect reward was calculated as follows: timestamp to enter the reward port location– timestamp of selection. We used a t-test to compare the response and reward latencies between correct and incorrect trials.

Surgery. Animals were premedicated with diazepam (2-5 mg/kg; i.p.), glycopyrrolate (0.05 mg/kg; s.c.), carprofen (5 mg/kg; s.c.), and butorphanol tartrate (0.5 mg/kg; s.c.) to counteract respiratory effects of anesthesia, to control pain, and to decrease risk of seizures. They were brought to a surgical level of anesthesia with isofluorane (1.0 – 2.5%). Using a stereotaxic apparatus (Kopf, Tujunga, CA), rats were unilaterally implanted with a custom hyperdrive into the DPPC (AP – 4.2 mm, ML ± 2.0 mm, DV – 0.1mm), and VPPC (AP – 5.2 mm, ML ± 4.5mm, DV – 2.0 mm). The hyperdrive had fifteen microdrives, each consisting of a drivable screw with guide tubing containing one stereotrode. Stereotrodes were made of two 12 μm twisted, formvar-insulated nichrome wires (A-M systems, Sequim, WA). A full turn of the screw advanced the stereotrode by 350 μm. Two silver ground wires were wrapped around anchor screws in the skull. The hyperdrive was secured to the skull by the ground screws, small anchor screws, grip cement (Dentsply Caulk, Milford, DE), and dental cement (Coltene/Whaledent Inc., Cuyahoga Falls, OH).

Histology. After the last recording session, the rats were deeply anesthetized with an overdose of Beuthanasia-D (100 mg/kg, i.p.) and the final recording site was marked with an electrolytic lesion. The rats were then perfused with normal saline, followed by 4% formalin. The brains were post-fixed for 24 hours in 4% formalin and then transferred to a 30% sucrose solution until the time for sectioning. The brains were sectioned at 40 μm and stained for Nissl material with thionin.

Single neuron recording. Neuronal activity recorded from stereotrodes, was amplified with a 2X gain 31-channel wireless head stage (Triangle BioSystems Inc., Durham, NC). Signals were passed through a high-gain amplifier (total = 10000X, MAP system, Plexon, Inc., Dallas, TX). Single-unit activity was filtered between 0.8 - 6 Hz. The signal was then digitized at 40 kHz for single-unit activity. These signals were extracted through real-time thresholding (Sort Client, Plexon, Inc). The final waveforms were stored with timestamps of relevant events and position information for later analysis.

Single neuron activity analysis. Spikes associated with putative individual cells were isolated offline based on waveform characteristics and using a variety of partially-automated and manual techniques (Offline Sorter, Plexon, Inc.). The result was a dataset for each cell containing timestamps corresponding to spike times and behaviorally relevant event markers. These datasets were further analyzed using Neuroexplorer (NEX, Nex Technologies, Colorado Springs, CO) , SPSS (IBM Corporation, Somers, NY) and Matlab (Mathworks, Natick, MA). Each cell was analyzed for behavioral correlates using two methods. The primary method was factorial analysis of variance (fANOVA), and we then confirmed the results with the bootstrapping approach described below. We analyzed two epochs from each completed trial: pre-stimulus and post-stimulus epochs were the 500 msec periods immediately before and after stimulus onset. Entry of the ready position of the other side of bowtie maze triggered the next trial. Rats invariably approached and checked the food port even after incorrect trials. Firing rate

was the dependent variable for the fANOVAs. For each neuron, we first computed the mean firing rate (spikes/sec) for each epoch on each trial. In the first set of analyses, the between-trial variable was outcome (correct response vs. incorrect response), and the within-trial variable was stimulus onset (pre-stimulus vs. post-stimulus). Level of significance for fANOVA was $p < 0.05$. To confirm the results of the first series of analyses (fANOVAs), we used a bootstrapping procedure. For each cell in each recorded session, we randomly shuffled the firing rates for epochs analyzed across all trials 1000 times to create 1000 shuffled datasets. For example, if the pre-stimulus epoch was the epoch under analysis and there were 100 trials, the 100 firing rates for the pre-stimulus epoch were shuffled to create one new dataset, and this was done 1000 times. We then compared the original F value to the F values from the shuffled datasets. The cell was considered to be selective if the observed F value was higher than 95% of the distribution of the F values from the shuffled datasets.

In the second set of analyses, to further understand changes of neuronal activity over time, a sliding window analysis was employed. We focused on the neuronal activity during the stimulus presentation period. For each neuron, we took a 100 ms window of time, beginning at stimulus onset and compared the mean firing rate of this 100 ms bin to the neuron's mean firing rate during pre-stimulus epoch by using paired t-test. We then advanced the window by 20 ms and analyzed the next 100 ms window of time, and continued until the end of the stimulus presentation. Significance of a cell was determined by at least two continuous bins showing statistically significant differences ($p < 0.05$).

Anatomical Results

Identification of Injection Sites

The site of a retrograde injection was defined as the area that encompassed the dye core and the region of necrosis surrounding it. The site of an anterograde injection was defined

as the region containing labeled cell bodies in the coronal section in which the area was largest. Cell counts were performed in the section where the spread of the injection site appeared largest. The estimated size of the injection sites and laminar location of the injection sites for each case are provided in Table 2. The locations of all injection sites analyzed are shown in Figure 4.

Figure 4

Borders of the PPC

The rostral border of the DPPC (~3.2-5.0 mm caudal to bregma) is largely consistent across previous studies (Reep *et al.* 1994; Swanson 2004; Paxinos and Watson 2005; Olsen and Witter 2016). There is less agreement, however, regarding the lateral and caudal extent of the region. For example, the caudal border has been variously placed at 6.1 mm posterior to the bregma (Paxinos and Watson 2014) and 6.9 mm posterior to the bregma (Swanson 2004, 2018). In addition, in Swanson (2018), VPPC is broader in the coronal plane. In our Nissl-stained sections, the caudal area of the PPC can be distinguished from adjacent visual and auditory cortices by characteristics of layers 4 and 5. Compared to adjacent visual and auditory areas, layer 4 contains is narrower. Cells in the layer 5 of the PPC are less densely packed than adjacent regions and has fewer large darkly staining pyramidal cells compared with adjacent regions. These cytoarchitectural features become less prominent about 6.3 mm posterior to the bregma where we place the caudal border. By our definition, VPPC is wider in the coronal plane than in Paxinos and Watson (2014) and narrower than in Swanson (2018) (Figure 1).

Figure 5

Projections from LPn to the PPC

The projection from the LPn to the PPC differs according to the rostrocaudal location of anterograde injection sites and subdivision of the LPn. The most rostral site, C13-090B was located in the ventrolateral subdivision of the laterodorsal nucleus of the thalamus near the rostrocaudal border with LPLR. This injection site may have also involved LPLR. Indeed, the patterns of labeling were similar to that arising from LPLR with the exception that we also observed labeling in the retrosplenial cortex. This was not observed for the other LPn injection sites. Case 13-053B, located entirely in LPLR, showed denser fiber labeling in the VPPC compared with DPPC (Table 3A, Figure 4A, and Figure 5C-D). This site targeted deeper layers of PPC. Injection sites for cases 13-052B and 13-054B were located at mid-rostrocaudal and caudal levels of LPMR, respectively (Figure 5A-B and E-F). Both cases showed labeled fibers throughout the entire PPC, but the more rostral case (13-052B) labeled DPPC more strongly and the caudal case (13-054B) labeled VPPC more strongly (Table 3A). In DPPC, the rostral site labeled PtPD more strongly and the caudal site labeled PtPR more strongly. The two most caudal cases, 13-089B and 13-091B involved both LPMR and LPMC with possibly some very small involvement of LPLR (Figure 4A). Like case 13-054B, these injection sites revealed stronger labeling in VPPC than in DPPC. The LPMR cases with and without LPMC involvement showed similar laminar patterns of labeling in PPC. The strongest labeling was in layers V and layers I.

Overall, LPLR preferentially targets deeper layers, whereas LPMR and LPMC preferentially target layers V and I. At least for injection sites in LPMR and LPMC, rostral sites target DPPC more strongly and caudal sites target VPPC more strongly.

Table 3

Projections between the PPC and POR

Retrograde tracer injections in POR resulted in fluorescently labeled cells in the PPC in all cases, though the density of labeling in PPC subdivisions differed based on the location of injection sites in the POR (Table 3B). In general, rostral POR is most heavily targeted by lateral and caudal portions of PPC. This is illustrated by comparing results of the ventrally located injection site 102FB (Table 3B; Figure 6A-B) with the dorsally located injection site, 98FB. Both cases displayed denser labelling in the VPPC (Table 3B; Figure 6C-D). This is especially true for the more caudally located injection sites (99FB in Table 3B; Figure 6E-F). The PPC projection to the POR originates in all layers except layer I. Based on densities of labeled cells, the projection to rostral POR is stronger from layer VI, especially from VPPC. In contrast, the projection to caudal POR from layer V is substantially stronger than that from layer VI.

Figure 6

All POR anterograde injection sites resulted in labeling in the PPC, regardless of the rostrocaudal location of the POR injection (Table 3C). Overall, POR projects more strongly to VPPC than to DPPC. There was a suggestion that caudal POR projects more heavily to PPC, in that case 40P resulted in a heavier density of labeled fibers compared to the rostral POR (case 39P) injections (Table 3B). The obvious heaviest density of labeled fibers was found in middle PtPD and PtPR (Figure 7C). In general, POR projects preferentially to layers VI and I, with a light projection terminating in layer V.

To summarize, PPC is reciprocally connected with the POR. POR targets VPPC more strongly than DPPC and the projections target VPPC projects more strongly to the POR than does the DPPC. Though weaker overall, rostral DPPC projects more strongly to rostral and

dorsal POR than to ventral and caudal POR. POR projections to VPPC than to DPPC are roughly equal in strength, though the projections arising from caudal POR may be stronger. The PPC projection to the POR is stronger from VPPC than from DPPC. The projections originate in all layers except layer I. Based on densities of labeled cells, the projection to rostral POR is stronger from layer VI, especially from VPPC. In contrast, the projection to caudal POR from layer V is substantially stronger than that from layer VI.

Figure 7

Electrophysiological Results

Behavior

Prior to surgery, rats were habituated to the behavioral room and apparatus, shaped on the VSA task, and then retrained on the task to a criterion of 70-80% accuracy. Accuracy was calculated as the number of correct trials divided by the number of correct trials plus the number of incorrect trials. Chance level of performance is 33.33%. After the implant surgery, rats were retrained on the task. Accuracy decreased after surgery, but improved across sessions. Mean accuracy across rats at the beginning of retraining was 45.0% (range 33.3%-55.6%). The animal that was at 33% in the first session was at 51% by the second session. Mean accuracy in the last sessions was 55.6% (range 45.0%-71.4%). The animal that was at 45% in the last session generally performed at about 50% accuracy. The mean accuracy across 42 recording sessions from 5 rats was is 51.01%, which allowed us to have almost equal numbers of correct and incorrect trials for the analyses. The mean omission rate (number of omission trials / total trials) was 26.4%. The response latency for correct trials was significantly faster than the response latency for incorrect trials. The means ± standard errors were 1.69 ± 0.07 sec for correct trials and 1.94 ± 0.06 sec for incorrect trials ($t(41) = 6.95$; $p < 0.001$). Likewise, the

latency to collect reward for correct trials was also significantly faster than the response latency for incorrect trials. The means ± standard errors were 2.30 ± 0.12 sec for correct trials and 3.68 ± 0.23 sec for incorrect trials ($t(41) = 6.77$; $p < 0.001$).

Figure 8

Histology

Examination of Nissl-stained coronal brain sections from each of the five animals indicated electrode tips located in DPPC were between 4.0-4.6 mm posterior to bregma and 2.0-4.0 mm lateral to the midline (Figure 8). Electrode tips located in VPPC were between 5.2-6.0 mm posterior to bregma and 6.0-7.0 mm lateral to the midline. Cells located in adjacent areas were not analyzed.

DPPC and VPPC cells signaled stimulus onset and predicted behavioral outcome

All five rats yielded isolated units. A total of 78 DPPC cells and 119 VPPC cells that had good quality waveforms and well isolated clusters were analyzed. Each cell was recorded for a single session. No cells were excluded from analysis. To investigate whether DPPC and VPPC cells signaled attention to visual stimuli, we first analyzed neuronal responses to stimulus onset by comparing firing rates for the 500 ms before vs 500 ms after the onset of the 500 ms target stimulus for correct vs incorrect trials. Of all DPPC cells, 24 (30.8%) showed selectivity for stimulus onset and/or outcome. Of all VPPC cells, 52 (43.7%) VPPC cells showed selectivity for stimulus onset and/or outcome. A total of 14 DPPC cells (17.95%) and 38 VPPC cells (31.9%) showed significant increases or decreases in firing rate associated with stimulus onset, alone (Table 4 and Figure 9). Thus, a significantly higher proportion of VPPC cells exhibited selectivity for stimulus onset compared with DPPC cells ($\chi^2_{(1)} = 4.74$, $p = 0.03$). Seven (9.0%) DPPC cells, and eight (6.7%) VPPC cells fired differentially depending on whether the animal was about to

make a correct selection. Three (3.9 %) DPPC cells and 6 (5.0%) VPPC cells exhibited a main effect of outcome alone. Thus, a total of 10 (12.8%) DPPC cells, and 14 (11.8%) VPPC cells fired differentially depending on the subsequent outcome of the trial.

Table 4

Figure 9

Sliding window analysis of neuronal activity during peri-stimulus epochs

Compared to the DPPC, the VPPC exhibited a significantly larger proportion cells showing selectivity of stimulus onset. To characterize changes in neuronal activity over time in DPPC and VPPC during the peri-stimulus epochs, we also used a sliding window analysis. For each neuron, we used a 100 ms sliding window, beginning at stimulus onset and advancing by 20 ms to the end of the stimulus presentation. Each window was compared with the neuron's mean firing rate during the pre-stimulus epoch using a paired t-test. The results showed that the firing rates of 32 (41.03%) DPPC cells and 102 (85.71%) VPPC cells were significantly different ($p < 0.05$) between pre-stimulus & post-stimulus epochs in at least two continuous sliding windows (Figure 10A). Compared to the DPPC, the VPPC had a significantly larger proportion of cells showing differential firing rate before and after stimulus onset ($\chi^2_{(1)} = 43.26$, $p < 0.01$). We also observed that VPPC cells showed selective activity for stimulus onset much earlier than DPPC cells. About half of VPPC cells (49.58%) displayed significantly different firing rates between pre-stimulus & post-stimulus epochs in the first two time bins immediately after stimulus onset. Figure 10B showed two example cells from the DPPC and VPPC. The VPPC cells (Figure 10B, Left) had significantly increasing activity immediately after stimulus onset; the DPPC cells

(Figure 10B, Right) had significantly increasing activity starting about 300ms after stimulus onset. The VPPC cells with fast onset were distributed across animals, sessions, and tetrodes. In addition, there were 18 groups (mostly pairs) of single units recorded in the same session on the same tetrode. Of those 18 groups, 13 showed heterogeneous latencies to signal stimulus onset. Only about 6% of DPPC cells showed selectivity in this window.

Figure 10

Discussion

In the present study, we used both neuroanatomical tract tracing methods and electrophysiological recordings in behaving animals to address the hypothesis that the rat PPC can be functionally and structurally differentiated. Based on cytoarchitectural characteristics and anatomical connections with LPn and POR, we concluded that the posterior border of the VPPC is more caudal than the definition in Paxino & Watson (2014), but does not extend to the most caudal portion of the PPC in Swanson (2018). The most caudal portion of the VPPC according to our definition is also a bit wider than the definition at the same level in Swanson (2018). Our simultaneous recordings in the DPPC and VPPC during performance on our VSA task revealed differential firing patterns across the two regions. More VPPC cells than DPPC cells were selective for stimulus onset. Moreover, VPPC cells became selective to stimulus onset earlier than DPPC cells. In addition to suggesting new borders for PPC in the rat, our data provide the first evidence for functional differentiation of the rat DPPC and VPPC.

In earlier studies, we reported the dense reciprocal connections between the PPC and the POR (Burwell and Amaral 1998a; Agster and Burwell 2009) and between the POR and thalamic nuclei (Agster *et al.* 2016; Tomás Pereira *et al.* 2016). The present study examined the

connections among various subdivisions of these structures in greater detail, providing a more comprehensive description of the connectivity, particularly with the LPn. Other studies have reported on the thalamocortical connections of the PPC, but these have not addressed the connections of the most caudal and lateral PPC (Hughes 1977; Chandler *et al.* 1992; Reep *et al.* 1994; Bucci et al. 1999; Kamishina et al. 2009; Wilber, Clark, Demecha*, et al.* 2014; Olsen and Witter 2016). Two recent studies reporting anatomical connections between the thalamic nuclei and PPC did address a more extended PPC, but did not include the caudolateral PPC as defined in the present study (Wilber, Clark, Demecha*, et al.* 2014; Olsen and Witter 2016). Wilber et al. (2014) reported significant differences of thalamic inputs between the medial and lateral portions of PPC but there was no differences between the rostral and caudal PPC. In this study, connectivity with the subdivisions of the LPn that was included in the analyses was only from the rostral LPn (LPMR and LPLR), but the input from the caudal LPn was lacking. Also, the caudal PPC that was defined in this study was the medial secondary visual cortex, which was different from the VPPC that we included in all our analyses. Another study from Olsen et al. (2016) carefully examined the PPC projections with the thalamus using both anterograde and retrograde injections in the PPC. They reported that dorsomedial PPC projects heavily to LPMR. The dorsolateral PPC projects to the posterior complex and less strongly to LPn. They found that the most lateral and caudal PPC projects only to the posterior complex. No subdivision of the PPC was found to project to the LPLR or the LPLC. Their retrograde labeling experiments showed that the LPMR projects more strongly to dorsomedial PPC than to dorsolateral PPC. However, they did not include any retrograde injections in the lateral and caudal PPC, so the retrograde labeling in the thalamus from the caudal portion of the PPC still needs to be clarified. Our current anterograde experiments covered the entire PPC with ventral extension that has not been fully reported in previous studies. Our data showed that the LPMR and LPMC project to both DPPC and VPPC consistent with classic nonspecific thalamocortical projections that

characteristically target layers I and V. In contrast, LPLR appears to target only deep layers in both subdivisions of the PPC.

Regarding the corticocortical connections, the PPC provides a strong projection to the POR, but the projection arising from the VPPC is stronger than that arising from the DPPC. DPPC projects to all rostrocaudal levels of POR. The projection originates in all cell layers, but the projections arising from layers V and VI are stronger. VPPC also projects to all rostrocaudal levels of POR. The projection originates in all cell layers, and overall, the projections arising from layers V and VI are stronger. However, layers II/III and VI from the VPPC project more strongly to rostral POR suggesting a feedforward or lateral pattern of projections (Felleman and Van Essen 1991). Interestingly, the rostral POR projects about equally to VPPC and DPPC, but caudal POR projects more strongly to both subregions. Also, the POR projections to PPC target layers I and VI suggesting a feedback projection. Unlike thalamocortical projections to thalamic relay nuclei, which arise predominantly in layer V, thalamocortical projections of associational regions like the PPC arise in both layers V and VI. One view of these projections to nonspecific thalamic nuclei is that layer V provides sensory or driver input to the thalamus and layer VI has modulatory impact over the driver inputs (Sherman 2016). If this is the case, then based on connectivity, the POR may play a role in modulating the PPC thalamocortical driver and modulator projections (Crandall et al. 2015).

Our anatomical findings provide further link for the rodent model of primate circuits that support visuospatial information processing. Here we have used a functional and comparative neuroanatomy structuralist regarding regarding homology, as opposed to the systematic biology or phylogenetic approach (Campbell and Hodos 1970). The monkey PPC, pulvinar, and PHC are considered the functional and connectional homologous structures of the rodent PPC, LPn and POR (Reep *et al.* 1994; Burwell *et al.* 1995; Kamishina *et al.* 2009; Zhou et al. 2017). As in the rodent brain, these structures exhibit substantial interconnectivity in the primate brain

(Baleydier and Mauguiere 1977; Baleydier and Mauguiere 1985, 1987; Cavada and Goldman-Rakic 1989; Suzuki and Amaral 1994b). Like the rat LPn, the monkey pulvinar provides substantial thalamic input to the entire PPC (Baleydier and Mauguiere 1977; Mesulam et al. 1977; Baleydier and Mauguiere 1987). Additionally, the monkey PHC, particular area TF, heavily interconnects with area 7 and lateral intraparietal area (LIP) of the PPC (Cavada and Goldman-Rakic 1989; Suzuki and Amaral 1994b). Our findings that the parietal connections with the rat LPn and POR parallel the interconnections of the monkey PPC, pulvinar, and PPC provide further evidence for functional and connectional homology across these brain structures in the rat and monkey.

To our knowledge, this is the first study to examine neuronal correlates of VPPC cells of visuospatial attention in rats. We used our novel VSA paradigm to further address the hypothesis that the rat PPC exhibits functional differentiation such that the DPPC is more involved in top-down attention and the VPPC is more involved in bottom-up attention. In the VSA task, rats were trained to monitor multiple spatial locations for the appearance of a visual stimulus and then to select a correct target for a food reward by approaching the spatial location in which the stimulus appeared. The rat must use attentional resources throughout a trial, beginning with stimulus-driven attention and ending with the use of prior knowledge to perform the appropriate behavioral response to gain the expected outcome.

Results from simultaneous recordings in DPPC and VPPC confirmed that both DPPC and VPPC are engaged in visuospatial attention. Our prior study showed that DPPC cells signal a variety of behavioral correlates consistent with top-down control in the translation of perception to action (Yang *et al.* 2017). In the present study, we compared neuronal correlates of DPPC with the VPPC. Interestingly, only 15-18% cells in DPPC were selective only for the onset of the visual stimulus In an analysis in which we compared neuronal activity in the pre-stimulus onset

epoch to the post-stimulus onset epoch only 15-18% cells in DPPC showed selectivity compared to 33% of VPPC cells (Table 4).

Using a sliding window analysis of the post-stimulus epoch, we found that VPPC cells exhibited much faster latencies to respond to stimulus onset than DPPC, consistent with a greater role in stimulus-driven attention (Figure 10). One possibility is that these VPPC cells with fast onset latencies were actually located in adjacent visual areas. We found, however, that these cells were distributed across animals, sessions, and tetrodes and were not preferentially located near borders with visual cortex. Importantly, pairs of single units recorded in the same session on the same tetrode showed heterogeneous latencies to respond to stimulus onset.

The sliding window analysis showed that, proportionately, twice as many VPPC neurons (85%) than DPPC neurons (41%) became selective within 500 ms of stimulus onset. Interestingly, the large majority of these cells in the VPPC (81%) became selective in under 150 ms post stimulus onset. In contrast, the majority of the DPPC cells (66%) became selective after 150 ms. This suggests that the VPPC is more involved in bottom-up attention, whereas the DPPC is involved in top-down attention. In other words, VPPC is responding preferentially to stimulus salience, whereas DPPC is providing a top-down signal based on task demands - in this case identifying the location of the stimulus. DPPC responses could also be signaling perceptual processes. Given that the stimuli all look exactly the same, however, we would argue that a top-down function is the more parsimonious interpretation.

Evidence from both psychophysiological and single-unit recording studies suggest that the response latencies associated with top-down attention are longer overall than those associated with bottom-up attention (Tomita et al. 1999; Buschman and Miller 2007; Li et al. 2010). Thus, a difference in neuronal response latencies in the VPPC compared to the DPPC could reflect a functional differentiation with regard to visuospatial attention. We observed that a number of cells in both DPPC (28.21%) and VPPC (44.54%) were responsive to stimulus onset or stimulus

onset and outcome. Moreover, cells in the rodent VPPC were more likely than DPPC to respond rapidly to the onset of a visual stimulus. These findings suggest that DPPC and VPPC interact closely in the service of visuospatial attention. Whereas the VPPC directly responds to target detection, the DPPC is also sensitive to the salience of possible targets that could perhaps become relevant signals to the future action selection or behavioral outcome. Interestingly, a population of cells in both DPPC and VPPC (12% in each region) fired differentially between correct and incorrect outcome, suggesting the two subregions of the PPC might interact during target selection. Although how DPPC and VPPC interact to process visuospatial information remains unclear, the POR, which has reciprocal connections with both DPPC and VPPC may be involved. Indeed, previous studies have shown the involvement of rodent POR in attentional monitoring (Bucci and Burwell 2004; Furtak *et al.* 2012). Thus, POR may participate in an attentional circuit that includes DPPC, VPPC, and the LPn.

A strength of our electrophysiological study was the use of a paradigm modeled after a task that has a long history in research on attention and executive control. We were able to measure many of the variables measured in the classic 5CSRT task, including accuracy and omissions as well as choice and reward latencies for correct and incorrect trials. One limitation of our study was that we were not able to measure impulsivity by estimating premature responses. This is because of the way animals were tracked during the variable delay. The variable delay was initiated when the rat's head entered a small window in the center of the maze, the ready position zone, facing toward the stimulus area. The delay was restarted when the rat's head moved out of the ready position zone. However, this could happen if the rat moved backward, forward, or simply checked the food port to the side. For that reason, we were unable to measure perseverative behavior, in this version of our task. Another limitation of our study is that our findings are correlational. Although we did not manipulate PPC activity in this study, we can use the task in the future for circuit analysis using optogenetic or chemogenetic methods.

To conclude, we provide anatomical and electrophysiological evidence that the rodent PPC can be functionally differentiated such that the DPPC supports top-down attention and the VPPC supports bottom-up attention. Our findings have a number of implications. For example, sensory information carried by thalamic inputs from the LPn could be further processed in the PPC. Our recent study has confirmed the role of the LPn in visuospatial attention using the VSA paradigm (Yang and Burwell 2020) together with the present study providing evidence to support the hypothesis of thalamo-cortical attention network. More detailed evidence is needed to understand the full mechanism. Also, the PPC connections with the POR may support a role for the POR in attentional monitoring of spatial context for changes (Bucci and Burwell 2004; Furtak *et al.* 2012). More generally, these findings indicate that research on the rodent PPC should include the ventral subdivision. Further research should use circuit analysis to further address how the PPC, LPn, and POR interact in the service of visuospatial attention.

Acknowledgements

This research was supported by the National Institute of Mental Health (R01-MH108729), the National Science Foundation (IOB-0522220 and IOB-1146334), and the Defense Advanced Research Projects Agency (N66001-10-C-2010).

References

Agster KL, Burwell RD. 2009. Cortical efferents of the perirhinal, postrhinal, and entorhinal cortices of the rat. Hippocampus. 19:1159-1186.

Agster KL, Burwell RD. 2013. Hippocampal and subicular efferents and afferents of the perirhinal, postrhinal, and entorhinal cortices of the rat. Behavioural Brain Research. 254:50-64.

Agster KL, Tomás Pereira I, Saddoris MP, Burwell RD. 2016. Subcortical connections of the perirhinal, postrhinal, and entorhinal cortices of the rat. II. efferents. Hippocampus.1213-1230.

Baldwin MKL, Balaram P, Kaas JH. 2017. The evolution and functions of nuclei of the visual pulvinar in primates. J Comp Neurol. 525:3207-3226.

Baleydier C, Mauguiere F. 1977. Pulvinar-latero posterior afferents to cortical area 7 in monkeys demonstrated by horseradish peroxidase tracing technique. Experimental Brain Research. 27:501-507.

Baleydier C, Mauguiere F. 1985. Anatomical evidence for medial pulvinar connections with the posterior cingulate cortex, the retrosplenial area, and the posterior parahippocampal gyrus in monkeys. The Journal of comparative neurology. 232:219-228.

Baleydier C, Mauguiere F. 1987. Network organization of the connectivity between parietal area 7, posterior cingulate cortex and medial pulvinar nucleus: a double fluorescent tracer study in monkey. Experimental Brain Research. 66:385-393.

Bari A, Dalley JW, Robbins TW. 2008. The application of the 5-choice serial reaction time task for the assessment of visual attentional processes and impulse control in rats. Nat Protoc. 3:759-767.

Bisley JW, Goldberg ME. 2003. Neuronal activity in the lateral intraparietal area and spatial attention. Science. 299:81.

Broussard JI, Sarter M, Givens B. 2006. Neuronal correlates of signal detection in the posterior parietal cortex of rats performing a sustained attention task. Neuroscience. 143:407-417.

Bucci DJ. 2009. Posterior parietal cortex: An interface between attention and learning? In. Neurobiology of Learning and Memory. p 114-120.

Bucci DJ, Burwell RD. 2004. Deficits in attentional orienting following damage to the perirhinal or postrhinal cortices. Behavioral Neuroscience. 118:1117-1122.

Bucci DJ, Conley M, Gallagher M. 1999. Thalamic and basal forebrain cholinergic connections of the rat posterior parietal cortex. NeuroReport. 10.

Burwell RD. 2001. Borders and cytoarchitecture of the perirhinal and postrhinal cortices in the rat. The Journal of Comparative Neurology. 437:17-41.

Burwell RD, Amaral DG. 1998a. Cortical afferents of the perirhinal, postrhinal, and entorhinal cortices of the rat. The Journal of Comparative Neurology. 398:179-205.

Burwell RD, Amaral DG. 1998b. Perirhinal and postrhinal cortices of the rat: Interconnectivity and connections with the entorhinal cortex. The Journal of Comparative Neurology. 391:293-321.

Burwell RD, Witter MP, Amaral DG. 1995. Perirhinal and postrhinal cortices of the rat: A review of the neuroanatomical literature and comparison with findings from the monkey brain. Hippocampus. 5:390-408.

Buschman TJ, Miller EK. 2007. Top-down versus bottom-up control of attention in the prefrontal and posterior parietal cortices. Science. 315:1860.

Campbell CB, Hodos W. 1970. The concept of homology and the evolution of the nervous system. Brain Behav Evol. 3:353-367.

Carli M, Robbins TW, Evenden JL, Everitt BJ. 1983. Effects of lesions to ascending noradrenergic neurones on performance of a 5-choice serial reaction task in rats; implications for theories of dorsal noradrenergic bundle function based on selective attention and arousal. Behavioural Brain Research. 9:361-380.

Caspari N, Arsenault JT, Vandenberghe R, Vanduffel W. 2017. Functional smilarity of medial superior parietal areas for shift-selective attention signals in humans and monkeys. Cerebral Cortex. 28:2085-2099.

Cavada C, Goldman-Rakic PS. 1989. Posterior parietal cortex in rhesus monkey: I. Parcellation of areas based on distinctive limbic and sensory corticocortical connections. The Journal of Comparative Neurology. 287:393-421.

Chandler HC, King V, Corwin JV, Reep RL. 1992. Thalamocortical connections of rat posterior parietal cortex. Neuroscience Letters. 143:237-242.

Chen LL, Lin LH, Green EJ, Barnes CA, McNaughton BL. 1994. Head-direction cells in the rat posterior cortex. I. Anatomical distribution and behavioral modulation. Exp Brain Res. 101:8-23.

Colby CL, Goldberg ME. 1999. Space and attention in parietal cortex. Annual Review of Neuroscience. 22:319-349.

Cook EP, Maunsell JHR. 2002. Attentional modulation of behavioral performance and neuronal responses in middle temporal and ventral Intraparietal areas of macaque monkey. The Journal of Neuroscience. 22:1994.

Corbetta M, Kincade JM, Ollinger JM, McAvoy MP, Shulman GL. 2000. Voluntary orienting is dissociated from target detection in human posterior parietal cortex. Nature Neuroscience. 3:292-297.

Corbetta M, Shulman GL. 2002. Control of goal-directed and stimulus-driven attention in the brain. Nature Reviews Neuroscience. 3:201-215.

Crandall SR, Cruikshank SJ, Connors BW. 2015. A corticothalamic switch: controlling the thalamus with dynamic synapses. Neuron. 86:768-782.

Felleman DJ, Van Essen DC. 1991. Distributed hierarchical processing in the primate cerebral cortex. Cereb Cortex. 1:1-47.

Furtak SC, Ahmed OJ, Burwell RD. 2012. Single neuron activity and theta modulation in postrhinal cortex during visual object discrimination. Neuron. 76:976-988.

Furtak SC, Cho CE, Kerr KM, Barredo JL, Alleyne JE, Patterson YR, Burwell RD. 2009. The Floor Projection Maze: A novel behavioral apparatus for presenting visual stimuli to rats. Journal of Neuroscience Methods. 181:82-88.

Furtak SC, Wei SM, Agster KL, Burwell RD. 2007. Functional neuroanatomy of the parahippocampal region in the rat: The perirhinal and postrhinal cortices. Hippocampus. 17:709-722.

Gottlieb J. 2007. From thought to action: the parietal cortex as a bridge between perception, action, and cognition. Neuron. 53:9-16.

Hughes HC. 1977. Anatomical and neurobehavioral investigations concerning the thalamo-cortical organization of the rat's visual system. The Journal of Comparative Neurology. 175:311-335.

Jacobson TK, Ho JW, Kent BW, Yang FC, Burwell RD. 2014. Automated visual cognitive tasks for recording neural activity using a Floor Projection Maze. Journal of Visual Experimentation.

Kaas JH, Baldwin MKL. 2019. The Evolution of the Pulvinar Complex in Primates and Its Role in the Dorsal and Ventral Streams of Cortical Processing. Vision (Basel). 4.

Kamishina H, Conte WL, Patel SS, Tai RJ, Corwin JV, Reep RL. 2009. Cortical connections of the rat lateral posterior thalamic nucleus. Brain Research. 1264:39-56.

Kravitz DJ, Saleem KS, Baker CI, Mishkin M. 2011. A new neural framework for visuospatial processing. Nature Reviews Neuroscience. 12:217-230.

Li L, Gratton C, Yao D, Knight RT. 2010. Role of frontal and parietal cortices in the control of bottom-up and top-down attention in humans. Brain Research. 1344:173-184.

Mesulam M-M, Van Hoesen GW, Pandya DN, Geschwind N. 1977. Limbic and sensory connections of the inferior parietal lobule (area PG) in the rhesus monkey: A study with a new method for horseradish peroxidase histochemistry. Brain Research. 136:393-414.

Nakamura H, Hioki H, Furuta T, Kaneko T. 2015. Different cortical projections from three subdivisions of the rat lateral posterior thalamic nucleus: a single-neuron tracing study with viral vectors. European Journal of Neuroscience. 41:1294-1310.

Nitz D. 2009. Parietal cortex, navigation, and the construction of arbitrary reference frames for spatial information. In. Neurobiology of Learning and Memory. p 179-185.

Nitz D. 2012. Spaces within spaces: rat parietal cortex neurons register position across three reference frames. Nature Neuroscience. 15:1365-1367.

Nitz D. 2014. The posterior parietal cortex: Interface between maps of external spaces and the generation of action sequences. In: Derdikman D, Knierim JJ, editors. Space,Time and Memory in the Hippocampal Formation Springer Vienna p 27-54.

Olsen GM, Ohara S, Iijima T, Witter MP. 2017. Parahippocampal and retrosplenial connections of rat posterior parietal cortex. Hippocampus. 27:335-358.

Olsen GM, Witter MP. 2016. The posterior parietal cortex of the rat: architectural delineation and thalamic differentiation. Journal of Comparative Neurology. 524:3774-3809.

Paxinos G, Watson C. 2005. The rat brain in stereotaxic coordinates. Amsterdam: Elsevier Academic Press.

Paxinos G, Watson C. 2014. Paxino's and Watson's The rat brain in stereotaxic coordinates. Amsterdam: Elsevier Academic Press.

Petersen SE, Posner MI. 2012. The attention system of the human brain: 20 years after. In. Annual Review of Neuroscience: Annual Reviews. p 73-89.

Reep RL, Chandler HC, King V, Corwin JV. 1994. Rat posterior parietal cortex: topography of corticocortical and thalamic connections. Experimental Brain Research. 100:67-84.

Reep RL, Corwin JV. 2009. Posterior parietal cortex as part of a neural network for directed attention in rats. Neurobiology of Learning and Memory. 91:104-113.

Saalmann YB, Kastner S. 2011. Cognitive and perceptual functions of the visual thalamus. Neuron. 71:209-223.

Sherman SM. 2016. Thalamus plays a central role in ongoing cortical functioning. Nat Neurosci. 19:533-541.

Shomstein S. 2012. Cognitive functions of the posterior parietal cortex: top-down and bottom-up attentional control. Frontiers in Integrative Neuroscience. 6.

Suzuki WA. 1996. Neuroanatomy of the monkey entorhinal, perirhinal and parahippocampal cortices: Organization of cortical inputs and interconnections with amygdala and striatum. Seminars in Neuroscience. 8:3-12.

Suzuki WA, Amaral DG. 1994a. Perirhinal and parahippocampal cortices of the macaque monkey: Cortical afferents. The Journal of Comparative Neurology. 350:497-533.

Suzuki WA, Amaral DG. 1994b. Topographic organization of the reciprocal connections between the monkey entorhinal cortex and the perirhinal and parahippocampal cortices. The Journal of Neuroscience. 14:1856-1877.

Swanson LW. 2004. Brain maps: Structure of the rat brain. . In. A laboratory guide with printed and electronic templates for data, models and schematics, 3 ed. Amsterdam, The Netherlands: Elsevier

Swanson LW. 2018. Brain maps 4.0-Structure of the rat brain: An open access atlas with global nervous system nomenclature ontology and flatmaps. J Comp Neurol. 526:935-943.

Takahashi T. 1985. The organization of the lateral thalamus of the hooded rat. The Journal of Comparative Neurology. 231:281-309.

Tomás Pereira I, Agster KL, Burwell RD. 2016. Subcortical connections of the perirhinal, postrhinal, and entorhinal cortices of the rat. I. afferents. Hippocampus.n/a-n/a.

Tomita H, Ohbayashi M, Nakahara K, Hasegawa I, Miyashita Y. 1999. Top-down signal from prefrontal cortex in executive control of memory retrieval. Nature. 401:699-703.

Whitlock JR, Pfuhl G, Dagslott N, Moser MB, Moser EI. 2012. Functional split between parietal and entorhinal cortices in the rat. Neuron. 73:789-802.

Wilber AA, Clark BJ, Demecha AJ, Mesina L, Vos JM, McNaughton BL. 2014. Cortical connectivity maps reveal anatomically distinct areas in the parietal cortex of the rat. Frontiers in Neural Circuits. 8:146.

Wilber AA, Clark BJ, Forster TC, Tatsuno M, McNaughton BL. 2014. Interaction of egocentric and world-centered reference frames in the rat posterior parietal cortex. The Journal of Neuroscience. 34:5431-5446.

Yang F-C, Burwell RD. 2020. Neuronal activity in the rat pulvinar correlates with multiple higher-order cognitive functions. Vision. 4.

Yang F-C, Jacobson TK, Burwell RD. 2017. Single neuron activity and theta modulation in the posterior parietal cortex in a visuospatial attention task. Hippocampus. 27:263-273.

Zhou N, Maire PS, Masterson SP, Bickford ME. 2017. The mouse pulvinar nucleus: Organization of the tectorecipient zones. Visual Neuroscience. 34:E011.

Table 1. Nomenclature and Abbreviations

Regions	Abbreviations
laterodorsal nucleus	LD
lateral posterior nucleus	LPn
nucleus lateralis posterior pars rostromedialis	LPMR
nucleus lateralis posterior pars caudomedialis	LPMC
nucleus lateralis posterior pars lateralis	LPL
nucleus lateralis posterior pars rostralis	LPLR
nucleus lateralis posterior pars caudalis	LPLC
posterior parietal cortex	PPC
dorsal posterior parietal cortex	DPPC
ventral and caudal posterior parietal cortex	VPPC
medial parietal association cortex	MPtA
lateral parietal association cortex	LPtA
parietal cortex, posterior area, dorsal part	PtPD
parietal cortex, posterior area, rostral part	PtPR
parietal cortex, posterior area, caudal part	PtPC
entorhinal cortex	EC
perirhinal cortex	PER
postrhinal cortex	POR
ventral postrhinal cortex	PORv
dorsal postrhinal cortex	PORd
dorsal posthinal cortex, rostral part	rPORd
dorsal postrhinal cortex, caudal part	cPORd

Nomenclature is from Paxinos and Watson (2005).

Table 2. Description of injection sites for cases included in analyses

case	Type		Location	Layers	Size (μm)
13-052B	anterograde	BDA	LPMR/LPLR	n/a	200
13-053B	anterograde	BDA	LPLR	n/a	300
13-054B	anterograde	BDA	LPMR/LPMC	n/a	300
13-089B	anterograde	BDA	LD/LPLR	n/a	100
13-090B	anterograde	BDA	LPLR	n/a	200
13-091B	anterograde	BDA	LPLR	n/a	100
102FB*	retrograde	FB	Rostral POR	V	200
97FB*	retrograde	FB	Rostral POR	V	400
98FB*	retrograde	FB	Middle POR	I-VI	600
95DY*	retrograde	DY	Caudal POR	III-VI	400
99FB*	retrograde	FB	Caudal POR	I-V	500
100FB*	retrograde	FB	Caudodorsal POR	I-VI	500
83B*	anterograde	BDA	Rostral Dorsal POR	V-VI	500
39P*	anterograde	PHA-L	Rostral POR	I-IV	400
134B*	anterograde	BDA	Dorsal POR	I-VI	500
40P*	anterograde	PHA-L	Caudal POR	III-VI	500

*Animals previously reported in Burwell and Amaral, 1998a, 1998b. Size of injection is reported as the diameter of the injection site dye core. Abbreviations list: BDA: biotinylated dextran amine, DY: diamidino yellow, FB: fast blue, PHA-L: *Phaseolus vulgaris*-leucoagglutinin. Abbreviations for this and the following tables can be found in the list of abbreviations.

Table 3. Connectivity among DPPC, VPPC, LPn, and POR

3A. LPn anterograde cases, location of injection sites, and densities of labeled fibers in PPC						
Target	C13-090B	C13-053B	C13-052B	C13-054B	C13-089B	C13-091B
Region	LDVL/LPLR	LPLR	LPMR	LPMR	LPMR/LPMC	LPMR/LPMC
DPPC	++	++	++++	+++	+++	++
VPPC	+++	+++	++	++++	++++	++++

3B. POR retrograde cases, layer of injection sites, and densities of labeled cells in PPC						
Target	102FB	97FB	98FB	95DY	100FB	99FB
Region	V	V	I-VI	III-VI	I-VI	I-V
DPPC	350	660	460	450	270	90
Layer II/III	376	617	288	438	240	59
Layer IV	268	136	664	329	457	230
Layer V	526	558	531	811	478	90
Layer VI	408	1283	481	561	117	58
VPPC	920	1020	730	1030	1050	920
Layer II/III	2187	1488	896	961	395	696
Layer IV	905	345	652	871	3999	1114
Layer V	1941	851	1153	1516	1818	1508
Layer VI	3558	2154	485	970	252	431

3C. POR anterograde cases, layer of injection site, and densities of labeled fibers in PPC				
Target	83B	39P	134B	40P
Region	V-VI	I-IV	I-VI	III-VI
DPPC	++	+	++	+++
VPPC	++	++	++	+++

All injection sites are organized from rostral to caudal locations (see also Figure 4). Densities for anterograde tracers were quantified on scale of 0-5 and averaged across total area: +, 0.5-1.5; ++, 1.5-2.5; +++, 2.5-3.5; ++++, 3.5-4.5; +++++, 4.5-5.0. See text for details about the laminar patterns of labeling. Essentially, LPMR in the LPn preferentially targets DPPC and VPPC Layers I and V with much lighter labeling in remaining layers. LPLR preferentially targets DPPC and VPPC layers IV-V with scant labeling in layer I. LPLP targets layers II/III in CPPC more heavily than it targets layers II/III in VPPC. Caudal POR targets PPC more strongly than rostral POR and the projects preferentially target laters I and VI. For retrograde injections the density of labeled cells (cells/mm^3) is shown for each PPC subdivision and for each layer. The laminar location of the injection site in the POR is shown for each case. See Table 1 for abbreviations

Table 4. Numbers and percentage of cells selective for stimulus onset and outcome

Epoch	Correlate	DPPC (%) ANOVA	DPPC (%) Bootstrapping	VPPC (%) ANOVA	VPPC (%) Bootstrapping
Peri-Stimulus	Stimulus Only	12 (15.38)	14 (17.95)	39 (32.77)[#]	38 (31.93)*
	Stimulus and Outcome	7 (8.97)	7 (8.97)	8 (6.72)	8 (6.72)
	Outcome Only	3 (3.85)	3 (3.85)	6 (5.04)	6 (5.04)
	Total Selective Cells	22 (28.21)	24 (30.77)	53 (44.54)	52 (43.70)

Numbers and percentage of selective cells. Numbers of the criterion cells for each analysis and numbers/percentages of cells that displayed significant main effects or interactions during behaviorally relevant epochs. A total of 78 DPPC cells and 119 VPPC cells were included in the analyses. The table summarizes the number of cells that exhibited significant selectivity in each analysis. Results from both the original fANOVA and the bootstrapping procedure are shown. For fANOVA analyses, significant level was $p < 0.05$. For the bootstrapping procedure, the 95th percentile was the cutoff for selectivity. * Significantly higher number of selective cells in VPPC than selective cells in DPPC ($\chi^2_{(1)} = 4.74$, $p = 0.03$). [#] Significantly higher number of selective cells in VPPC than selective cells in DPPC ($\chi^2_{(1)} = 6.55$, $p = 0.01$).

Figures and Captions

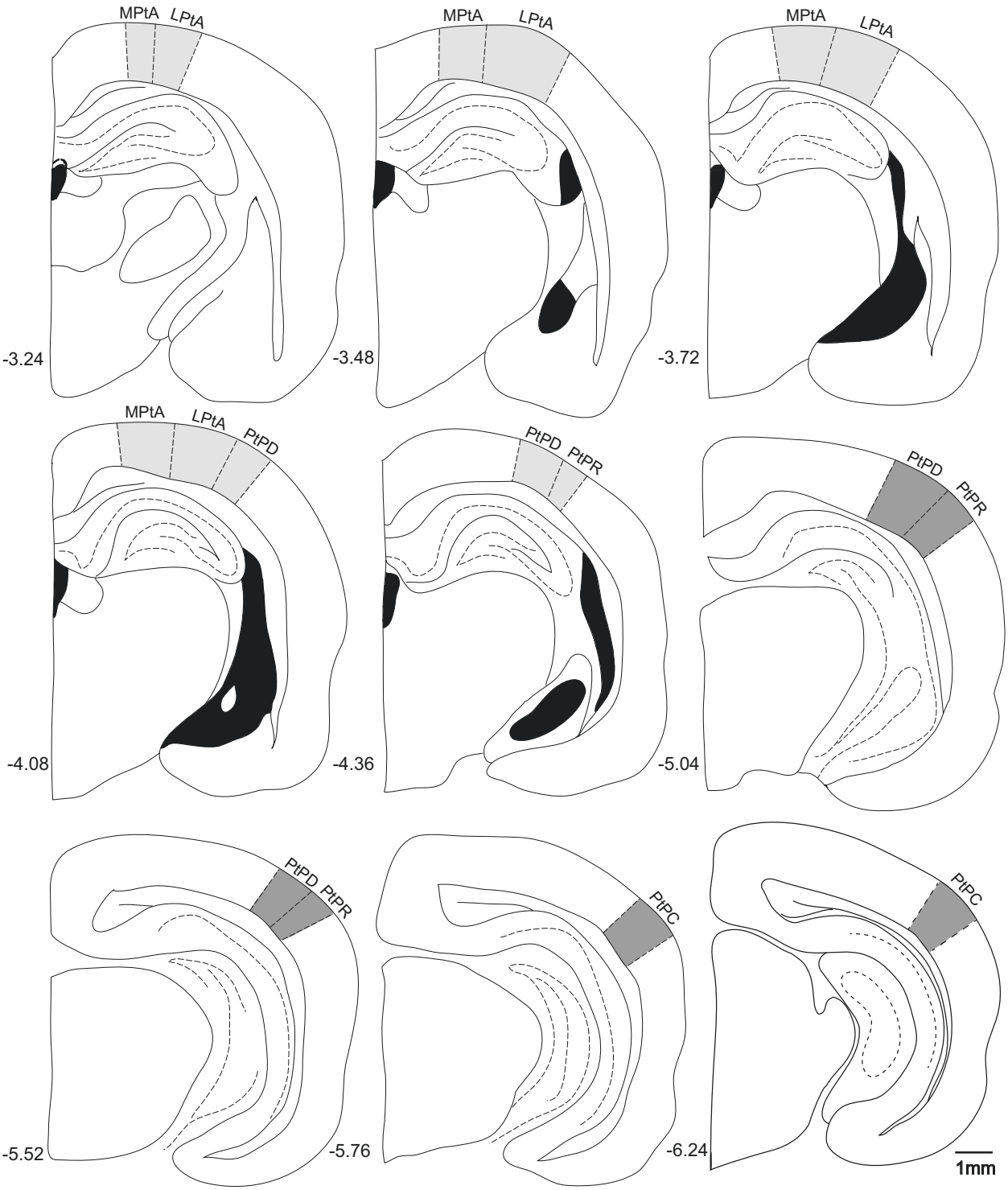

Figure 1. Coronal sections through posterior parietal cortex (PPC) in the rat. Subdivisions according to Paxinos & Watson (2005) include medial parietal association cortex (MPtA), lateral parietal association cortex (LPtA), and parietal cortex, posterior area, dorsal part (PtPD); rostral part (PtPR); caudal part (PtPC). Dorsal PPC and ventral PPC are shown in lighter grey and darker grey, respectively.

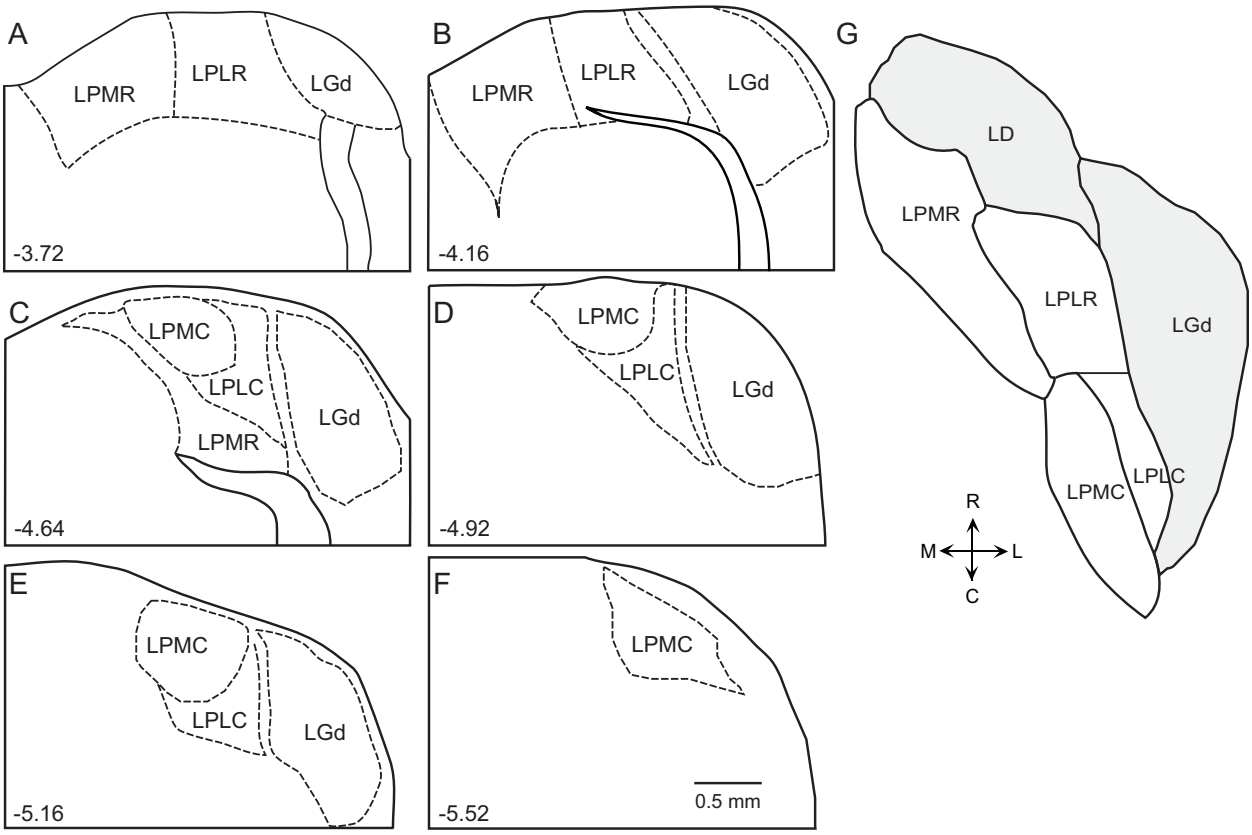

Figure 2. The lateral posterior nucleus of the thalamus (LPn). A-F. Subdivisions of the LPn adapted from Paxinos and Watson (2014) are shown in coronal section through the right hemisphere of the rat brain. G. Subdivisions are shown in a schematic of the flattened right hemisphere LPn in the transverse plane (from above). The lateral dorsal nucleus (LD) and the dorsal part of the lateral geniculate nucleus (LGd) are shown for reference. Other abbreviations: LPMR, nucleus lateralis posterior pars rostromedialis; LPMC, nucleus lateralis posterior pars caudomedialis; LPL, nucleus lateralis posterior pars lateralis.

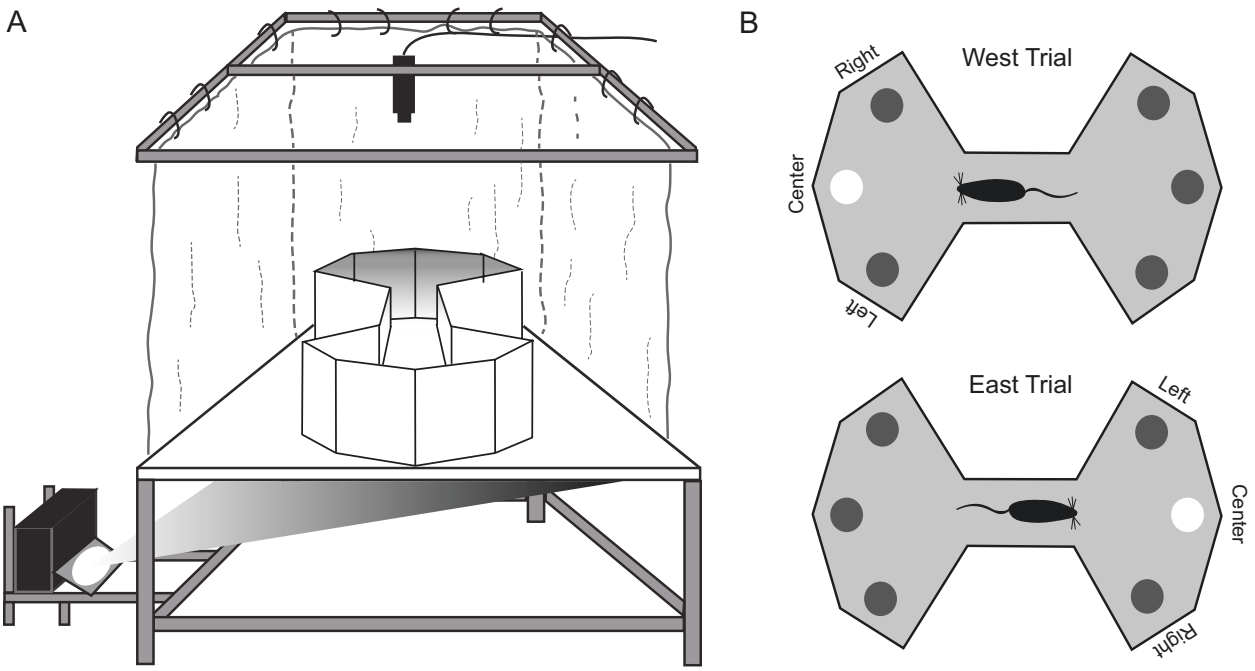

Figure 3. The Visuospatial Attention (VSA) task. A. Schematic of the Floor Projection Maze with the bowtie-shaped enclosure used for the task. B. Top-down view of west vs. east trials. Trials were initiated when the rat stopped in the ready position (middle of the maze) and faced one side of the maze (either west or east). After a variable period, the target location was briefly illuminated. The animal made a selection by approaching one of the three locations in the same side, and then returned to the food port for a food reward. After the animal consumed the reward, a new trial from the alternative side would be triggered immediately.

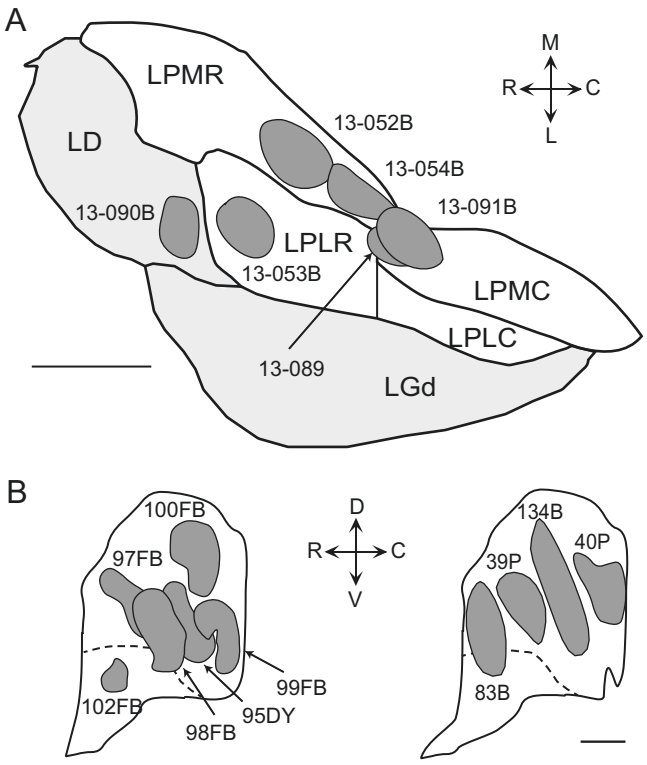

Figure 4. Tract tracer injection sites. A. Location of thalamic anterograde sites are shown in a flattened transverse map of the LPn. B. Locations of cortical retrograde (left) and anterograde (right) sites are shown in flattened maps of the POR. Dorsal and ventral POR are demarcated by dashed lines. See Table 1 for abbreviations. Scale bars are 0.5 mm.

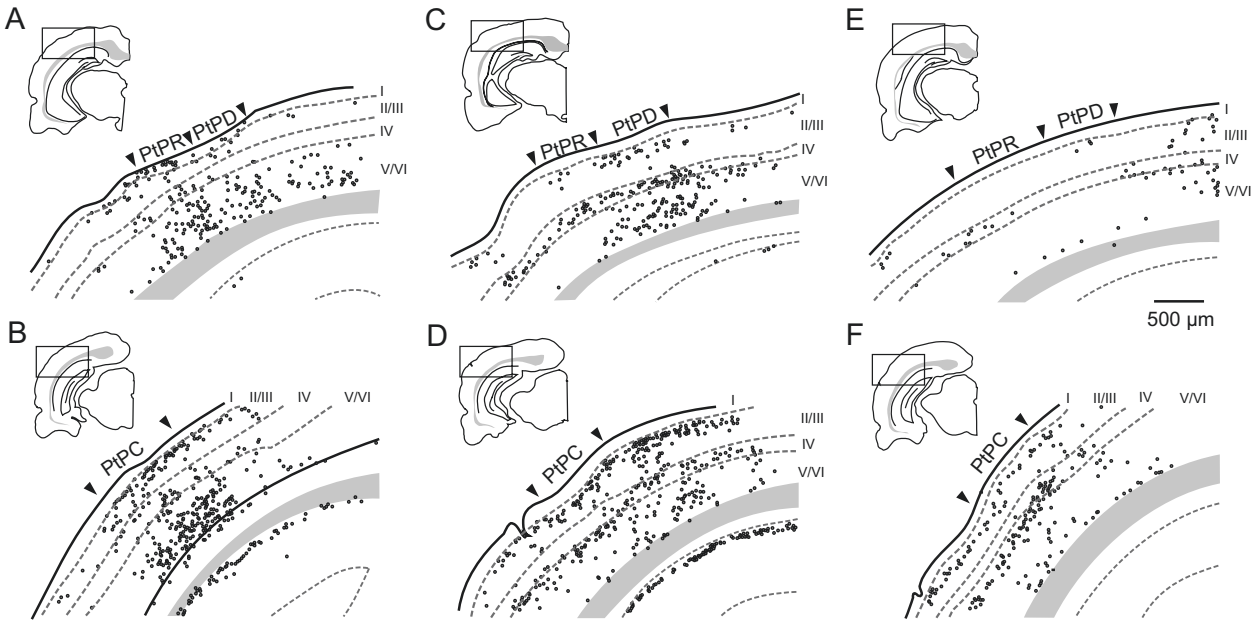

Figure 5. Anterograde labeling in the PPC arising from tracer injections in the LPn. The upper and lower panels showed labeling throughout the dorsal DPPC and ventral posterior parietal cortex (DPPC and VPPC, respectively). A-B. Representative case 13-052B whose injection site was located in the LPMR showed the densest labeling in the DPPC and much weaker labeling patterns in the VPPC. C-D. Representative case 13-053B whose injection site was located mainly in LPLR showed poor labeling in DPPC and denser labeling in VPPC. E-F. Representative case 13-054B whose injection site was in the caudal part of the LPMR and most rostral part of LPMC had dense labeling throughout the entire PPC. Panels A, C, and E show levels at -4.2, -4.8, and -4.3 mm relative to bregma, respectively. Panels B, D, and F show level -5.7 mm relative to bregma. Scale bar shown is 500 µm.

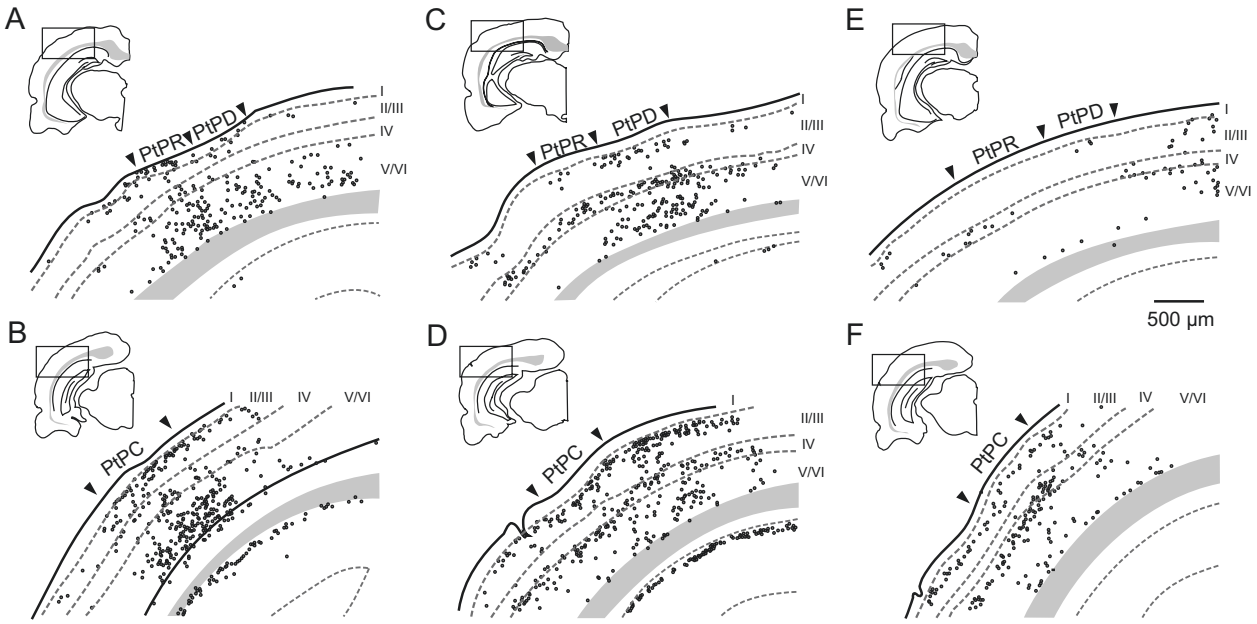

Figure 6. Schematic of the retrogradely labeled cells in the PPC arising from injection in the POR. The upper and lower panels showed labeling throughout the dorsal and caudal posterior parietal cortex (DPPC and VPPC, respectively). A-B. Representative case 102FB (left) whose injection site was located in the deep layers of rostral POR showed weak to moderate labeling in the DPPC. Denser labeled cells were found in the VPPC. C-D. Representative case 98FB (middle) whose injection site was located in all layers of mid rostra-caudal POR had labeled cells throughout entire PPC with heavier labeling in the more caudal sections. E-F. Representative case 99FB (right), whose injection site was located in layer I-V of caudal POR, resulted in poor labeling in the DPPC and dense labeling in the VPPC. Scale bar shown is 500 µm.

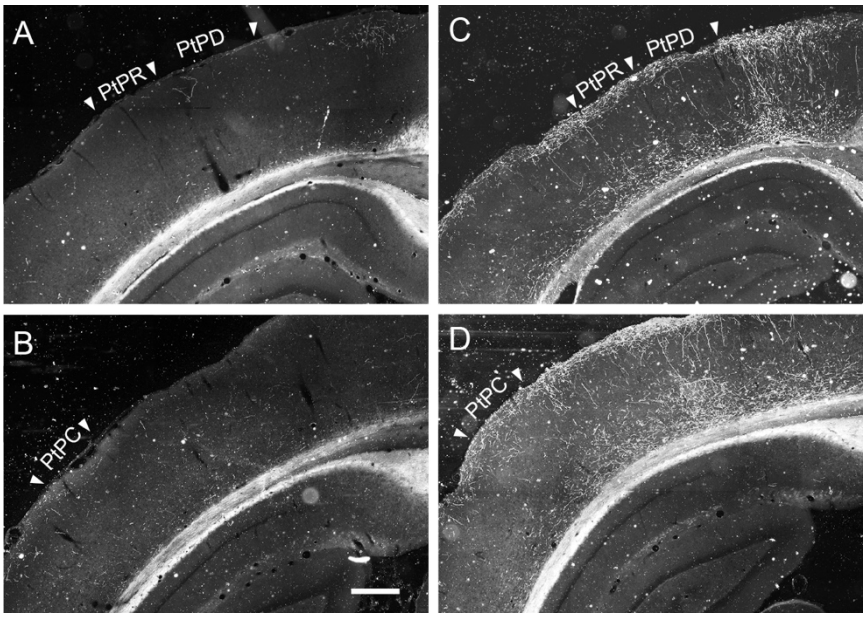

Figure 7. Anterograde labeling in the PPC arising from the injection in the POR. The upper and lower panels showed labeling throughout the dorsal and ventral posterior parietal cortex (DPPC and VPPC). Representative case 39 (left) whose injection site was located in the rostral POR showed poorly labeling in the DPPC. Weak to moderate labeling was observed in the VPPC. Representative case 40 (right) whose injection site was located in the caudal POR displayed moderate to dense labeling throughout the entire PPC, especially in middle PtPR and PtPD. Scale bar shown is 500 μm.

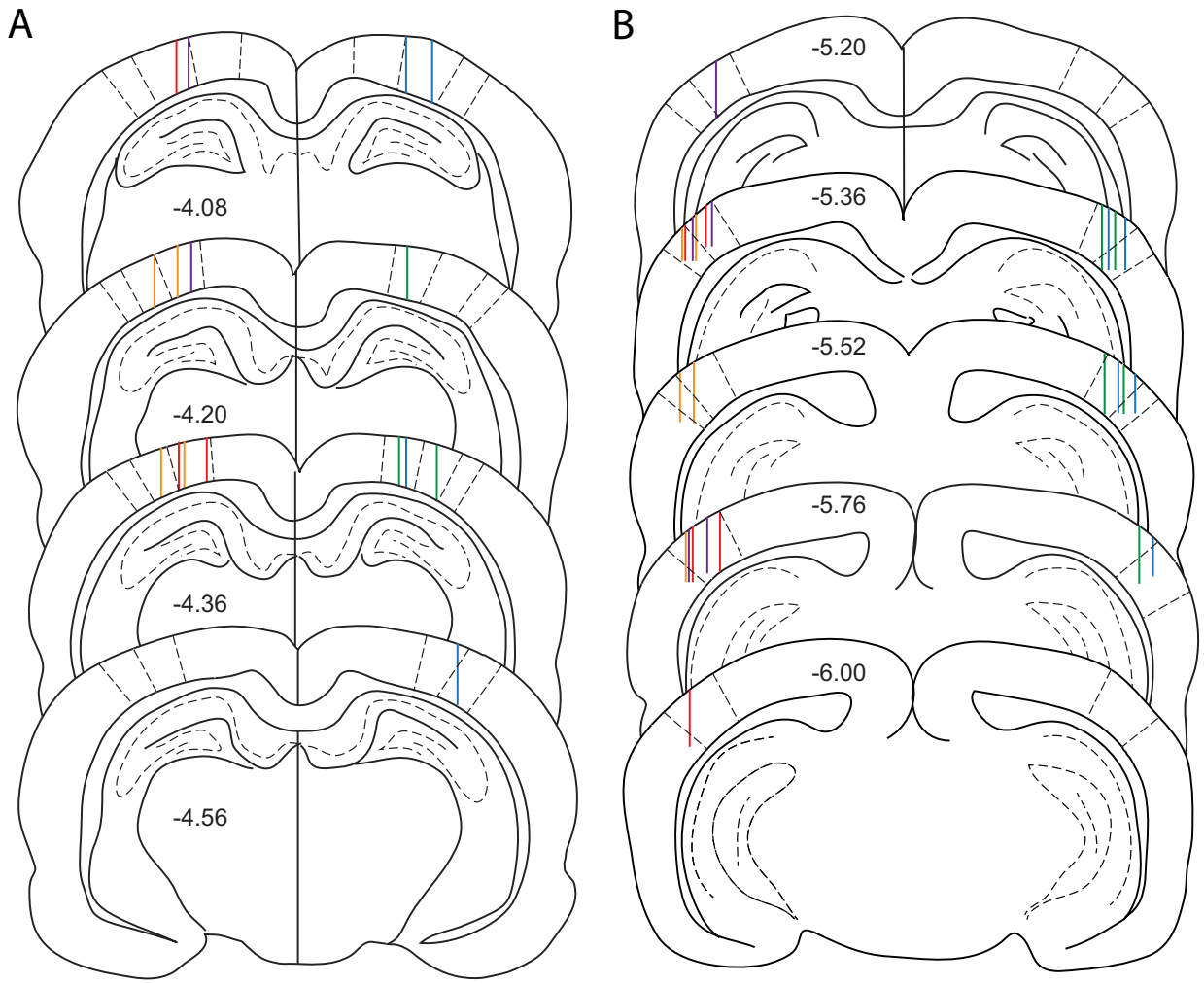

Figure 8. Estimated locations of implanted stereotrodes in DPPC (A) and VPPC (B). Numbers on each coronal section indicate mm from bregma. Stereotodes from each animal are shown in a different color. See Figure 1 for PPC subdivisions.

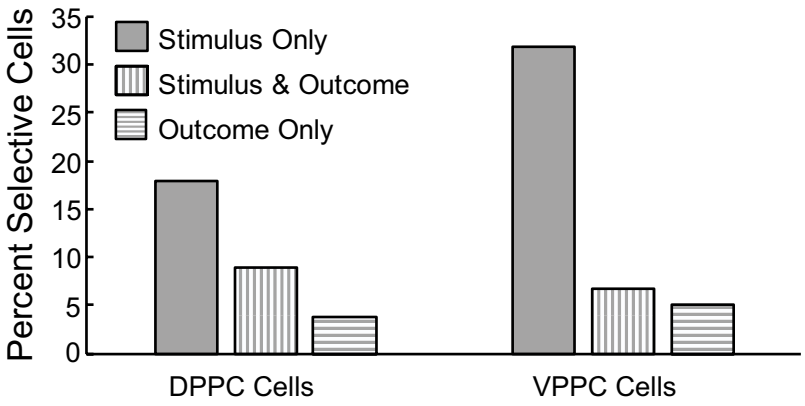

Figure 9. Correlates of selective DPPC and VPPC cells. Shown are percentages of cells selective for stimulus onset, outcome, or both. VPPC show disproportionate responses to stimuli only as compared with the VPPC. Light and dark bars indicate percentages of cells in the DPPC and VPPC, respectively.

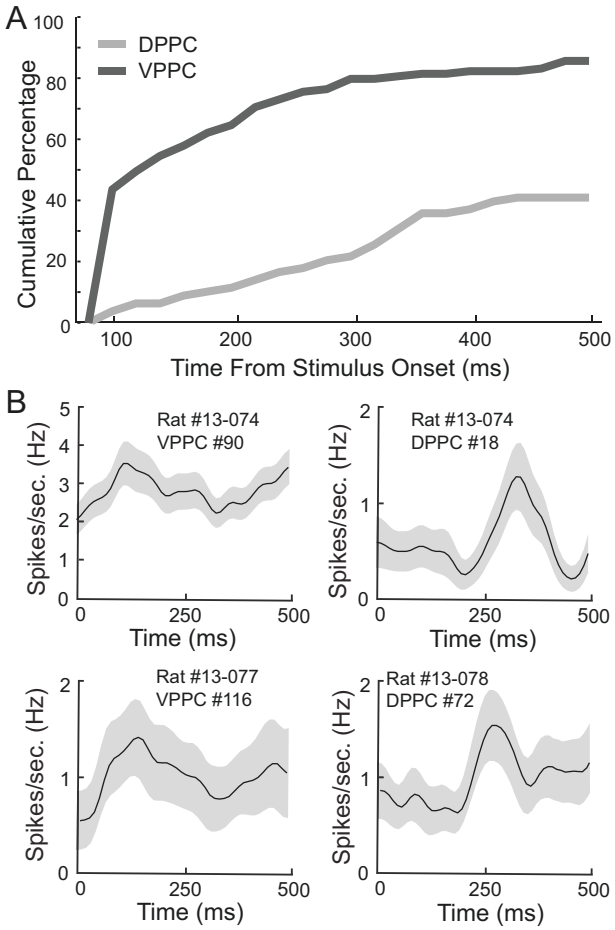

Figure 10. VPPC cells show faster latencies to respond to stimulus onset. A. Cumulative percentage of cells that exhibited a significant difference between PreStimulus and PostStimulus epochs in in 100 ms windows sliding by 20 ms. Light and dark grey lines indicate cumulative percentage of significant cells in the DPPC and VPPC, respectively. B. Single neuron examples showing mean firing rate (solid lines) and standard error (shaded) from stimulus onset in DPPC (Right) and VPPC (Left), respectively. Time 0 is the start of stimulus onset. The VPPC cells (Left) had significantly increasing activity immediately after stimulus onset; the DPPC cells (Right) had significantly increasing activity starting about 300ms after stimulus onset.